THEORETICAL AND APPLIED MECHANICS
Article in Press (2024) DOI: https://doi.org/10.2298/TAM241203010K

THEORETICAL AND EXPERIMENTAL INVESTIGATIONS OF THE CONTROLLED MOTION OF A ROLLER RACER

Alexander A. Kilin, Tatiana B. Ivanova, Yury L. Karavaev, and Kirill S. Yefremov

Abstract. In this paper, we address the problem of the controlled motion of a roller racer on a plane. We assume that the angle between the platforms is a given periodic function of time (control function), and the no-slip conditions (nonholonomic constraint) and viscous friction forces act at the points of contact of the wheels with the plane. In this case, all trajectories of the reduced system tend asymptotically to a periodic solution. In this paper, we show that for a selected periodic control function, there exists a motion of the system that is bounded (along a circle) and unbounded (along a straight line). An unbounded motion corresponds to the resonant case which takes place at zero average value of the control function. The theoretical dependence of the trajectory and the velocity of the roller racer on its parameters and the parameters of the selected control function is investigated. These dependences are confirmed experimentally.

Introduction

In this paper, we address the problem of the controlled motion of a roller racer. The roller racer is a system consisting of two platforms connected to each other (by means of a cylindrical hinge). The platforms can freely rotate in the horizontal plane independently of each other. Each platform has a wheel pair that is rigidly fastened to it and consists of two wheels lying on the same axis, which can freely rotate independently of each other. The forward motion of the roller racer is enabled by periodic oscillations of the platforms relative to each other.

In describing the dynamics of the system, we assume that there is no slipping at the points of contact of the wheels with the plane. In this case, each wheel pair can be replaced with a knife edge, which is located at its center of mass and prohibits sliding in the direction perpendicular to the plane of the wheels. The equivalence of such systems is shown in [1] using a vehicle with two rotating symmetric wheel

2020 *Mathematics Subject Classification:* 37J60, 70E60.
Key words and phrases: roller racer, nonholonomic constraint, viscous friction, control, periodic solution.

pairs as an example. The no-slip condition and the replacement of the wheel pair with a knife edge are also used in investigating the dynamics of a roller racer (a wheeled vehicle with fastened wheel pairs) in [2, 3], a wheeled vehicle with two rotating wheel pairs (snakeboard) in [4–6], and in investigating wheeled vehicles consisting of three and more platforms (a literature review can be found in [7, 8]).

Classical papers on the dynamics of wheeled vehicles include [9–12]. These studies are concerned with various models of a motor vehicle with a fastened rear axle (the model of a platform with two wheel pairs, one of which is fastened) and the simplest two-link vehicles. The dynamics of a snakeboard is explored in [13–18].

In the most general case, the *free* dynamics of a roller racer is investigated in [2]. Equations of motion on a plane are obtained and it is shown that, in the general case, the motion relative to a fixed coordinate system is asymptotic: except for the straight-line motion, the trajectories tend to circles and the motion is bounded. The asymptotic stability of straight-line motions for the case where the center of the system's mass is at the point of attachment of the platform is analyzed in [12].

In [3,19–22] the *controlled* motion of a roller racer is investigated. It is assumed that the angle between the platforms (the control function) is a given periodic function of time. In [3] it is shown that a periodic change in the angle can lead to unbounded acceleration. It is proved that, in the general case, in the presence of viscous friction forces at the point of contact of the wheels with the plane (see also [19]), there is no constant acceleration. In [20, 22], the controlled motion of the roller racer is considered taking into account Coulomb's friction between the wheels and the plane of motion. In [21] it is assumed that each of the two platforms of the roller racer additionally has a rotor whose angular velocity is a given periodic function of time. It is shown that, in this case, it is possible to achieve acceleration at which the velocity of the system increases as $t^{1/3}$ and the system moves on average along a strip bounded by two straight lines.

We also mention the studies [23,24] concerned with the controlled motion of the roller racer performed by the periodic displacement of one or several point masses, located on the leading platform, relative to the symmetry axis of this platform.

A comparison of theoretical and experimental results on the controlled motion of the roller racer in the case of straight-line motion with viscous friction is presented in [25, 26].

In [3] it is proved that in the case of viscous friction and a periodic control function all trajectories of the reduced system tend asymptotically to a periodic solution. In this paper, we carry out a theoretical and experimental investigation of the trajectories of the roller racer which correspond to these periodic solutions, depending on the control parameters and the mass-geometric characteristics of the system.

This paper is structured as follows. In Section 1 we specify the main design features and the assumptions under which the dynamics of the roller racer is examined and the corresponding equations of motion are derived. In Section 2 we analyze the steady-state periodic regime of motion, to which all motions of the roller racer tend asymptotically. Possible trajectories of the system and conditions for their existence are described. In Section 3 we give examples of periodic control

functions and the corresponding bounded and unbounded trajectories of the point of connection of the platforms of the roller racer to each other. In Section 4 we analyze the dependence of the average velocity of motion of the roller racer along a straight line on the control parameters and the mass-geometric characteristics of the roller racer. In Section 5 we present a comparison of the theoretical and experimental results obtained for the motion of the roller racer along a straight line and along a circle.

1. Equations of motion

Consider the problem of a roller racer moving on a plane. The roller racer consists of two platforms connected to each other (by means of a cylindrical hinge), which can freely rotate in the horizontal plane independently of each other (see Fig. 1). Each platform has a wheel pair rigidly fastened to it and consisting of two wheels lying on the same axis and rotating independently of each other. The forward motion of the roller racer is enabled by periodic oscillations of the platforms relative to each other.

A scheme of the roller racer on the plane is shown in Fig. 1, in which the following notation is used: P is the point of connection of the platforms to each other, A_1 and A_2 are the positions of the centers of mass of the first and the second platform, and C_1 and C_2 are the positions of the centers of mass of the corresponding wheel pairs. The notation of the main quantities used in this paper is presented in Table 1.

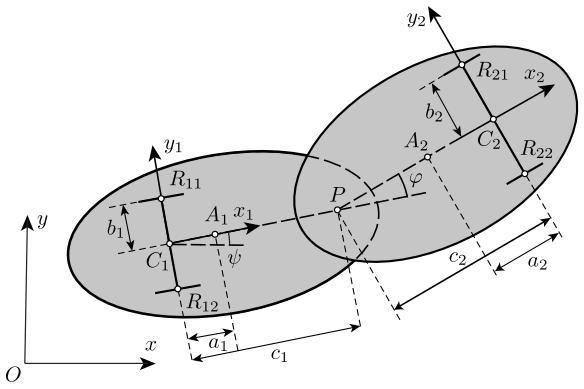

FIGURE 1. The roller racer on a plane

To analyze the dynamics of the system, we define three coordinate systems:

— an *inertial* coordinate system Oxy in which the plane Oxy coincides with the plane of motion (Fig. 1);

— a *noninertial* coordinate system $C_1x_1y_1$ rigidly fastened to *the first platform*, with origin C_1 at the center of mass of the wheel pair. We direct the axes C_1x_1 and C_1y_1, respectively, along the tangent and the normal to the plane of the wheels;

TABLE 1. Symbols

φ	the angle between the axes C_1x_1 and C_2x_2 (the orientation of the platforms relative to each other)
ψ	the angle between the axes Ox and C_1x_1 (the orientation of the first platform relative to the fixed coordinate system)
$\boldsymbol{r} = (x, y)$	the radius vector of the point of attachment of the platforms, P, in the fixed coordinate system Oxy
c_1, c_2	distances from the center of the first and the second wheel pair to point P
a_1, a_2	distances from point C_1 to the center of mass of the first platform and from point C_2 to the center of mass of the second platform
m_1, m_2	the masses of the first and the second platform
I_{10}, I_{20}	the moments of inertia of the first and the second platform relative to their centers of mass (points A_1 and A_2)
I_1, I_2	the moments of inertia of the first and the second platform relative to point P
κ_1, κ_2	coefficients of viscous friction of the first and the second platform
b_1, b_2	distances from the point of contact of the wheels to the center of mass of the corresponding wheel pair
h_1, h_2	the radius of the wheels on the first and the second platform

— a *noninertial* coordinate system $C_2x_2y_2$ rigidly fastened to *the second platform*, with origin C_2 at the center of mass of the wheel pair, and with the axes directed along the tangent and the normal to the plane of the wheels.

We specify the main design features and the assumptions under which we examine the dynamics of the roller racer.

— Assume that the center of mass of the first and the second platform (points A_1 and A_2) lie, respectively, on the axes C_1x_1 and C_2x_2 (see Fig. 1).
— The orientation angle φ of the platforms relative to each other is a given *periodic* function of time (with period T).
— As the roller racer moves, there is no slipping at the points of contact of the wheels with the plane.

In [1] it is shown that, in wheeled vehicles of the type considered here, each wheel pair can be replaced with a weightless knife edge which is located at its center of mass and prohibits sliding in the transverse direction (relative to the plane of the wheels).

Thus, the configuration space $\mathcal{N}_{\boldsymbol{q}}$ of the system under consideration is defined by the generalized coordinates $x(t)$, $y(t)$, $\psi(t)$, which specify the position of point P

and the orientation of the first platform relative to the fixed coordinate system Oxy:

$$\mathcal{N}_{\boldsymbol{q}} = \{\boldsymbol{q} = (x, y, \psi), \psi \mod 2\pi\} \approx \mathbb{R}^2 \times \mathbb{S}^1.$$

We will describe the dynamics of the system by the quasi-velocities $\boldsymbol{v} = (v_1, v_2)$ and ω, where $\boldsymbol{v}$ is the velocity of point P referred to the moving coordinate system $C_1x_1y_1$, and ω is the absolute angular velocity of the first platform. The quasi-velocities are related to the generalized velocities by

$$v_1 = \dot{x}\cos\psi + \dot{y}\sin\psi, \quad v_2 = -\dot{x}\sin\psi + \dot{y}\cos\psi, \quad \omega = \dot{\psi}. \tag{1.1}$$

The angles of rotation of the wheels relative to their axes $\phi_{ij}(i, j = 1, 2)$ can be recovered, if necessary, by the integration of equations [1, 3]:

$$\begin{aligned} &h_1\dot{\phi}_{11} = b_1\dot{\psi} - \dot{x}\cos\psi - \dot{y}\sin\psi, \quad h_1\dot{\phi}_{12} = -b_1\dot{\psi} - \dot{x}\cos\psi - \dot{y}\sin\psi, \\ &h_2\dot{\phi}_{21} = b_2(\dot{\varphi}(t) + \dot{\psi}) - \dot{x}\cos(\varphi(t) + \psi) - \dot{y}\sin(\varphi(t) + \psi), \\ &h_2\dot{\phi}_{22} = -b_2(\dot{\varphi}(t) + \dot{\psi}) - \dot{x}\cos(\varphi(t) + \psi) - \dot{y}\sin(\varphi(t) + \psi). \end{aligned} \tag{1.2}$$

Nonholonomic constraints expressing the absence of slipping at the points of contact of the wheels have the form [3]:

$$f_1 = v_2 - c_1\omega = 0, \quad f_2 = -v_1\sin\varphi(t) + v_2\cos\varphi(t) + c_2(\omega + \dot{\varphi}(t)) = 0. \tag{1.3}$$

The kinetic energy of the entire system can be represented as

$$\begin{aligned} T = \frac{1}{2}M(v_1^2 + v_2^2) + m_1(a_1 + c_1)v_2\omega + \frac{1}{2}I_1\omega^2 + \frac{1}{2}I_2(\dot{\varphi}(t) + \omega)^2 \\ + m_2(a_2 - c_2)(v_2\cos\varphi - v_1\sin\varphi)(\dot{\varphi}(t) + \omega), \end{aligned}$$

where $M = m_1 + m_2$ is the mass of the entire system.

To investigate the influence of the friction force on the dynamics of the roller racer, we will consider the simplest model of viscous friction [19, 27]. Suppose that the forces of viscous friction with the Rayleigh function act at the points of contact of the wheels with the plane:

$$R = \frac{1}{2}\left(\kappa_1\dot{\phi}_{11}^2 + \kappa_1\dot{\phi}_{12}^2 + \kappa_2\dot{\phi}_{21}^2 + \kappa_2\dot{\phi}_{22}^2\right),$$

where $\dot{\phi}_{ij}(i, j = 1, 2)$ are the angular velocities of rotation of the wheels. Taking into account relations (1.1), (1.3) and the quadratures for the angular velocities of rotation of the wheels (1.2), the Rayleigh function written in terms of quasi-coordinates has the form

$$R = \mu_1(b_1^2\omega^2 + v_1^2) + \mu_2(b_2^2(\dot{\varphi}(t) + \omega)^2 + (v_1\cos\varphi + v_2\sin\varphi)^2), \tag{1.4}$$

where $\mu_1 = \kappa_1/h_1^2$, $\mu_2 = \kappa_2/h_2^2$ are the reduced viscose friction coefficients.

Remark 1.1. The proposed model describes the rolling friction torques and the viscous friction torques which arise in bearings as the wheels rotate on their axes. Incorporation of such a friction torque does not lead to violation of the no-slip condition. A similar friction torque which does not violate the no-slip condition was considered in the Chaplygin sphere rolling problem [28].

The equations of motion taking into account the constraints (1.3) and the friction forces described by the Rayleigh function (1.4) can be written as [1, 3]:

$$\begin{aligned}
\frac{d}{dt}\Big(\frac{\partial T}{\partial v_1}\Big) - \omega\frac{\partial T}{\partial v_2} &= \sum_{i=1}^{2}\lambda_i\frac{\partial f_i}{\partial v_1} - \frac{\partial R}{\partial v_1},\\
\frac{d}{dt}\Big(\frac{\partial T}{\partial v_2}\Big) + \omega\frac{\partial T}{\partial v_1} &= \sum_{i=1}^{2}\lambda_i\frac{\partial f_i}{\partial v_2} - \frac{\partial R}{\partial v_2},\\
\frac{d}{dt}\Big(\frac{\partial T}{\partial \omega}\Big) + v_1\frac{\partial T}{\partial v_2} - v_2\frac{\partial T}{\partial v_1} &= \sum_{i=1}^{2}\lambda_i\frac{\partial f_i}{\partial \omega} - \frac{\partial R}{\partial \omega},
\end{aligned} \tag{1.5}$$

where λ_1 and λ_2 are undetermined multipliers.

To calculate the undetermined multipliers, we solve the constraints (1.3) relative to the velocities ω and v_2 and differentiate them with respect to time. Then, we substitute the resulting dependences $\dot v_2(v_1, \dot v_1, t)$ and $\dot\omega(v_1, \dot v_1, t)$ into the last two equations of the system (1.5). Solving the resulting equations, we obtain the dependence of the undetermined multipliers on $v_1, \dot v_1$ and time. We do not present here the explicit expressions for $\lambda_{1,2}(v_1, \dot v_1, t)$ since they are fairly cumbersome.

Remark 1.2. The constraints (1.3) can be solved for the velocities ω and v_2 under the condition

$$c_1\cos\varphi + c_2 \neq 0. \tag{1.6}$$

Condition (1.6) is satisfied for any control function $\varphi(t)$ at $c_1 > c_2$. If $c_1 \leqslant c_2$, then in defining the control function it is necessary to choose its parameters in such a way that condition (1.6) is always satisfied. Or it is necessary to choose from the very beginning other quasi-velocities for describing the dynamics of the roller racer. This can always be done, for example, by changing the numbering of the platforms.

Substituting the resulting undetermined multipliers into the first of equations (1.5), we obtain the following equation governing the evolution of the translational velocity v_1 of the first platform:

$$\dot v_1 = \big(A(t) - C(t)\big)v_1 + B_1(t) + B_2(t) - D(t), \tag{1.7}$$

where

$$\begin{gathered}
A(t) = -\frac{\dot\varphi\sin\varphi(J_1S_2 + \delta S_1)}{S_1(J_1\sin^2\varphi + MS_1^2)}, \quad B_1(t) = \frac{\ddot\varphi\sin\varphi(J_1c_2 - J_2S_1)}{(J_1\sin^2\varphi + MS_1^2)}\\
B_2(t) = \frac{\dot\varphi^2(J_1c_1c_2\sin^2\varphi - S_1(c_1\delta\cos\varphi - \varepsilon c_2S_1))}{S_1(J_1\sin^2\varphi + MS_1^2)}\\
C(t) = 2\frac{(b_1^2\mu_1 + b_2^2\mu_2)\sin^2\varphi + \mu_1S_1^2 + \mu_2S_2^2}{J_1\sin^2\varphi + MS_1^2},\\
D(t) = 2\frac{\dot\varphi\sin\varphi\big(c_1\mu_2(b_2^2 - c_2^2)\cos\varphi - c_2(b_1^2\mu_1 + c_1^2\mu_2)\big)}{J_1\sin^2\varphi + MS_1^2},\\
S_1 = c_1\cos\varphi + c_2, \quad S_2 = c_1 + c_2\cos\varphi.
\end{gathered}$$

Here, to abbreviate the formulae, we introduce the following notation:

$$\delta = c_1a_2m_2 + c_2a_1m_1, \qquad \varepsilon = m_1a_1 + c_1m_2,$$
$$J_1 = I_{10} + I_{20} + m_1a_1^2 + m_2(a_2^2 + c_1^2 - c_2^2), \qquad J_2 = I_{20} - m_2(c_2^2 - a_2^2).$$

Expressing the velocity v_2 from the first of the constraint equations (1.3) and substituting it into relations (1.1), we obtain the following system of equations on the configuration space $\mathcal{N}_{\mathbf{q}}$:

$$\begin{aligned} \dot\psi &= \frac{v_1\sin\varphi(t) - c_2\dot\varphi(t)}{c_1\cos\varphi(t) + c_2},\\ \dot x &= v_1\cos\psi - c_1\frac{v_1\sin\varphi(t) - c_2\dot\varphi(t)}{c_1\cos\varphi(t) + c_2}\sin\psi,\\ \dot y &= v_1\sin\psi + c_1\frac{v_1\sin\varphi(t) - c_2\dot\varphi(t)}{c_1\cos\varphi(t) + c_2}\cos\psi. \end{aligned} \tag{1.8}$$

The resulting system of equations (1.7)–(1.8) describes the behavior of the roller racer in the case where the angle $\varphi(t)$ between the platforms is a given function of time.

In this case, the nonautonomous equation (1.7) governing the evolution of velocity v_1 decouples from the system (1.7)–(1.8). Thus, the reduced system reduces to one nonautonomous linear differential equation whose solution depends on the form of the control function and the parameters of the roller racer.

2. Analysis of the steady-state regime of motion

Let us write equation (1.7) for brevity as

$$\dot v_1 = -\Phi(t)v_1 + \Psi(t), \tag{2.1}$$

where $\Phi(t), \Psi(t)$ are functions which for the case of T-periodic control functions $\varphi(t)$ are also periodic with the same period T.

In [3] it is proved that in this case the following statement holds.

PROPOSITION 2.1. *For the positive coefficients (of friction) $\mu_1 > 0$ and $\mu_2 > 0$, equation (2.1) has a particular time-periodic solution $v_1 = Q(t)$ to which all trajectories of this equation tend asymptotically as $t \to +\infty$. The solution $Q(t)$ is given by:*

$$Q(t) = \frac{1}{P(t)}\left(\frac{1}{(P(T)-1)}\int_0^T \Psi(\tau)P(\tau)d\tau + \int_0^t \Psi(\tau)P(\tau)d\tau\right),$$

where

$$P(t) = \exp\left(\int_0^t \Phi(\tau)d\tau\right).$$

The particular time-periodic solution $v_1 = Q(t)$ corresponds to the steady-state motion of the roller racer. Next, we analyze the trajectories of the point of attachment of the platforms relative to the fixed coordinate system during the steady-state motion depending on the parameters of the control function.That is

to say, assume that

$$v_1(t) = Q(t).$$

To analyze the position and orientation of the system, we make use of a complex representation for the configuration variables (x, y). In order to do this, we introduce a new variable

$$Z(t) = x(t) + iy(t).$$

The system of equations (1.8) can be written as

$$\dot{\psi} = F_T(t), \quad \dot{Z} = e^{i\psi(t)}\big(Q(t) + ic_1F_T(t)\big), \tag{2.2}$$

where $F_T(t)$ is a bounded function which is also T-periodic for T-periodic control functions $\varphi(t)$:

$$F_T(t) = \frac{Q(t)\sin\varphi(t) - c_2\dot{\varphi}(t)}{c_1\cos\varphi(t) + c_2}, \quad F_T(t) = F_T(t+T). \tag{2.3}$$

As is well known, the general solution of equation (2.2) for the function $\psi(t)$ is represented in this case as

$$\psi(t) = \Omega_\psi t + \psi_T(t) + \psi_0, \tag{2.4}$$

where Ω_ψ is a constant which is defined as the average over a period of the function $F_T(t)$, $\psi_T(t)$ is a T-periodic function with zero average (over period T), and ψ_0 is a constant:

$$\begin{aligned}
\Omega_\psi &= \langle F_T\rangle = \frac{1}{T}\int_0^T F_T(\tau)d\tau,\\
\psi_T &= \int_0^t (F_T(\tau) - \Omega_\psi)d\tau - \frac{1}{T}\int_0^T d\tau\int_0^\tau (F_T(z) - \Omega_\psi)dz,\\
\psi_0 &= \psi(0) + \frac{1}{T}\int_0^T d\tau\int_0^\tau (F_T(z) - \Omega_\psi)dz.
\end{aligned} \tag{2.5}$$

Substituting (2.4) into the equation for $\dot{Z}$ in (2.2) and making elementary transformations, we obtain

$$\dot{Z} = e^{i(\Omega_\psi t + \psi_0)}H_T(t), \tag{2.6}$$

where $H_T(t) = e^{i\psi_T(t)}(Q(t) + ic_1F_T(t))$ is a bounded T-periodic function. We represent it as a Fourier series expansion:

$$H_T = \sum_{k\in\mathbb{Z}} A_k e^{i\Omega kt}, \quad \Omega = \frac{2\pi}{T}, \tag{2.7}$$

where A_k are (complex) constants, coefficients of expansion of the function H_T:

$$A_k = \frac{1}{T}\int_0^T H_T(\tau)e^{-i\Omega k\tau}d\tau.$$

Substituting the expansion (2.7) into the equation for $\dot{Z}$ (2.6), we obtain

$$\dot{Z} = e^{i\psi_0}\sum_{k\in\mathbb{Z}} A_k e^{i(\Omega_\psi + \Omega k)t}. \tag{2.8}$$

To define the trajectory of the point of attachment P of the platforms relative to the fixed coordinate system, we integrate (2.8). The result of this integration depends on whether there exists a k such that the argument of the exponential function in (2.8) vanishes. We single out two cases in which the behavior of the system will be qualitatively different.

(1) Nonresonant case: $\Omega_\psi + \Omega k \neq 0$ for all $k \in \mathbb{Z}$.
(2) Resonant case: there exists a $k = k_*$ such that $\Omega_\psi + \Omega k_* = 0$.

Let us analyze the trajectories of the system in each of these cases.

2.1. Nonresonant case. Assume that *there does not exist a k such that* $\Omega_\psi + \Omega k = 0$. In this case, integrating equation (2.8), we obtain

$$Z(t) = Z(0) + e^{i\psi_0} \sum_{k\in\mathbb{Z}} \frac{-iA_k}{\Omega_\psi + \Omega k}(e^{i(\Omega_\psi+\Omega k)t} - 1). \tag{2.9}$$

Without loss of generality, we will assume that $Z(0) = 0$. Then, according to (2.9), in the reference frame that rotates about the point with the coordinates

$$Z_0 = e^{i\psi_0} \sum_{k\in\mathbb{Z}} \frac{iA_k}{\Omega_\psi + \Omega k} \tag{2.10}$$

with the angular velocity Ω_ψ, the trajectory of the point of attachment P of the platforms is a closed curve defined by the bounded T-periodic function

$$\tilde{Z}(t) = e^{i\psi_0} \sum_{k\in\mathbb{Z}} \frac{-iA_k}{\Omega_\psi + \Omega k} e^{i\Omega k t}. \tag{2.11}$$

In this case, the average value of the distance $\bar{R}$ from point P to Z_0 is defined as a zero harmonic of the series (2.11):

$$\bar{R} = \left|\frac{A_0}{\Omega_\psi}\right|, \quad A_0 = \frac{1}{T}\int_0^T H_T(\tau)d\tau. \tag{2.12}$$

In this case, $\bar{R}$ is the radius of the circle (with the center at point Z_0) along which point P moves on average in the absolute coordinate system Oxy. The average linear velocity of motion along this circle is

$$\bar{V} = \frac{\Omega_\psi T \bmod 2\pi}{T}\bar{R}. \tag{2.13}$$

In the fixed coordinate system the trajectory of point P can be closed or nonclosed, depending on the value of the ratio Ω_ψ/Ω.

1. If $\Omega_\psi/\Omega \in \mathbb{Q}$ is a rational number, i.e., if it can be represented as the ratio p/q, $p, q \in \mathbb{Z}$, $q \neq 1$, then the function $Z(t)$ is qT-periodic, the trajectory of point P becomes closed after q periods of control (examples of such trajectories are shown in Fig. 3a,b).
2. If $\Omega_\psi/\Omega \in \mathbb{R}\backslash\mathbb{Q}$ is an irrational number, then the trajectory of point P is a nonclosed curve consisting of equal segments traced out in period T, which, for each period, turn relative to the center Z_0 by angle $\Omega_\psi T$ (see Fig. 3c).

Let us formulate the results presented above in the form of the following statement.

PROPOSITION 2.2. *Let $\Omega_\psi + \Omega k \neq 0$ for all $k \in \mathbb{Z}$. Then the point of attachment P of the platforms moves on average in a circle of radius $\bar{R}$ (2.12) with the center at point Z_0 (2.10). If exist coprime integers $l, k \in \mathbb{Z}$, $(l \neq 1)$ such that $l\Omega_\psi + k\Omega = 0$, then the trajectory of point P is closed. Otherwise, point P moves along a bounded quasi-periodic curve.*

2.2. Resonant case. Assume that *there exists a $k = k_*$ such that $\Omega_\psi + \Omega k_* = 0$*. We will call this value k_* and the corresponding trajectory *resonant*.

In this case, we represent equation (2.8) as

$$\dot{Z} = e^{i\psi_0} A_{k_*} + e^{i\psi_0} \sum_{\substack{k\in\mathbb{Z},\\ k\neq k_*}} A_k e^{i(\Omega_\psi + \Omega k)t}, \tag{2.14}$$

where A_{k_*} is the expansion coefficient corresponding to $k = k_*$.

Integrating (2.14) gives

$$Z(t) = e^{i\psi_0} A_{k_*} t + e^{i\psi_0} \sum_{\substack{k\in\mathbb{Z},\\ k\neq k_*}} \frac{-iA_k}{\Omega_\psi + \Omega k}(e^{i(\Omega_\psi + \Omega k)t} - 1). \tag{2.15}$$

Thus, in contrast to the case discussed in Section 2.1, a term (linearly) growing with time appears in the function $Z(t)$ defining the trajectory of the point of attachment P of the platforms.

It follows from (2.15) that point P moves on average with the velocity

$$V_* = |A_{k_*}| \tag{2.16}$$

along a straight line in the direction

$$\psi_* = \psi_0 + \arg A_{k_*} \tag{2.17}$$

relative to the axis Ox. In this case, in the reference frame moving with velocity V_* in the direction ψ_*, the trajectory of the point of attachment P of the platforms is a closed curve defined by a bounded T-periodic function (see Fig. 5):

$$\tilde{Z}_*(t) = \sum_{\substack{k\in\mathbb{Z},\\ k\neq k_*}} \frac{-iA_k}{\Omega(k - k_*)} e^{i\Omega(k-k_*)t}. \tag{2.18}$$

The resonant expansion coefficient A_{k_*} depends on the parameters of the control function and the characteristics of the roller racer and can take zero value. In this case, the point P moves in a closed *bounded* trajectory (see Fig. 7) defined by the function

$$Z(t) = Z_0 + \tilde{Z}_*(t),$$

where Z_0 is defined by the sum (2.10) at all $k \neq k_*$.

Let us formulate the results presented above in the form of the following statement.

PROPOSITION 2.3. *Assume that there exist $k_* \in \mathbb{Z}$ for which $\Omega_\psi + \Omega k_* = 0$. Then*

— if the corresponding expansion coefficient is $A_{k_*} \neq 0$, the point of attachment P of the platforms moves without bound *on average along a straight line turned at angle ψ_* (2.17) relative to the axis Ox with the average velocity V_* (2.16);*

— if the corresponding expansion coefficient is $A_{k_*} = 0$, point P moves along a closed bounded trajectory defined by the function (2.18).

Next, we consider specific periodic control functions $\varphi(t)$ and give examples of resonant and nonresonant trajectories of the roller racer.

For numerical calculations we will use the following mass-geometric parameters of the roller racer which correspond to a full-scale specimen described below in Section 5, taking into account the relation between the mass-geometric characteristics of the platforms with wheel pairs and skates [1]:

$$\begin{gathered} m_1 = 0.647 \text{ kg}, \quad a_1 = 0.065 \text{ m}, \quad c_1 = 0.186 \text{ m}, \quad I_{01} = 0.0044 \text{ kg} \cdot \text{m}^2, \\ m_2 = 0.587 \text{ kg}, \quad a_2 = 0.0023 \text{ m}, \quad c_2 = 0.044 \text{ m}, \quad I_{02} = 0.0038 \text{ kg} \cdot \text{m}^2, \\ b_1 = b_2 = 0.0078 \text{ m}, \quad \mu_1 = \mu_2 = 0.3 \text{ kg/s}. \end{gathered} \tag{2.19}$$

The design of the roller racer allows changing the mass of the second platform by adding additional weights into special compartment symmetric relative to the center of mass of the second platform. Therefore, in analyzing the dependence of the velocity of the roller racer on the mass-geometric characteristics of the roller racer we will use different values of the parameters of the second platform which correspond to different numbers of additional weights.

3. Examples of steady-state motions

3.1. The choice of a control function. The orientation of the platforms of the roller racer relative to each other is defined by periodic function $\varphi(t)$ with some average value. Also, the rate of change in angle $\varphi(t)$ near this average value (the rapidity of relative motion) can be different, with the other control parameters (amplitude and period of motions) being constant.

Such controls can be modeled, for example, by the following continuous differentiable function, which will be considered as a control function in this paper:

$$\varphi(t) = \alpha \frac{2\pi}{T} \frac{\prod_{n=1}^{N}(2n+1)}{\prod_{n=1}^{N} 2n} \int \cos^{(2N+1)}\Big(\frac{2\pi t}{T}\Big) dt + \varphi_0, \tag{3.1}$$

where α, T and φ_0 are constants. The multipliers in front of the integral in (3.1) are defined in such a way that the maximal deviation of the function $\varphi(t)$ from φ_0 is equal to α and N is an integer defining the rapidity of motion. The larger N, the closer to the vertical the tangent to the function $\varphi(t)$ at $t = 0, T/2$, see Fig. 2. The case of the control function (3.1) with $N = 0$ (which is just a sine function) is discussed also in [3].

3.2. Bounded motion. Consider examples of trajectories of the roller racer which correspond to the control function (3.1) with parameters at which $\Omega_\psi + \Omega k \neq 0$ for $\forall\ k \in \mathbb{Z}$.

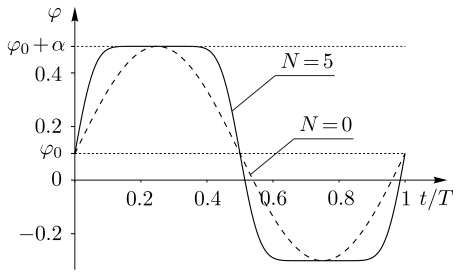

FIGURE 2. Graphs of the function $\varphi(t)$ for $N = 0$ and $N = 5$, $\alpha = 0.4$ rad, $\varphi_0 = 0.1$ rad

In this case, the point of attachment P of the platforms of the roller racer moves on average in a circle (see Proposition 2.2). The radius and the position of the center of the circle are determined from relations (2.10) and (2.12). The roller racer moves along this circle with the average linear velocity $\bar{V}$ (2.13). As examples, we show in Fig. 3a,b closed periodic trajectories for $N = 0$ and $N = 5$, and in Fig. 3c we show a quasi-periodic trajectory for $N = 0$. Figure 4 shows the dependences $\bar{V}$ (2.13) and $\bar{R}$ (2.12) on period T for different values of φ_0 and N and the corresponding trajectories of point P.

The graphs shown in the figure and the analysis of the quadratures (2.2) yield the following conclusions.

- An increase in the parameter φ_0 leads to a decrease in the radius of the circle along which point P moves on average, without significant changes in the velocity of motion along this circle. Hence, in Fig. 4a,d we show for each N only one dependence graph $\bar{V}(T)$ for $\varphi_0 = 0.2$ rad. The other graphs in the chosen scale have almost no differences from those presented in Fig. 4a,d.
- An increase in the period of control, T, leads to a decrease in the velocity of motion along the circle without significant changes in the radius of this circle.
- The value of $\bar{R}$ changes slightly with an increase in N and with other parameters fixed (see Fig. 4b,e with equal values of φ_0 and T), but the angular velocity $\bar{V}$ increases (see Fig. 4a,d with equal values of T), i.e., an increase in the rapidity of motion (the velocity of change of sign of the function $\varphi(t)$ in the middle of the period) leads to an increase in the velocity of motion along the circle.

3.3. Unbounded motion. Next, we consider examples of bounded and unbounded resonant trajectories of the roller racer in the case of control functions of the form (3.1).

In the general case, the search for the parameters of the control function which correspond to the resonant trajectory reduces to solving the equation (see Proposition 2.3)

$$\Omega_\psi(N, T, \alpha, \varphi_0) + 2\pi k_*/T = 0. \tag{3.2}$$

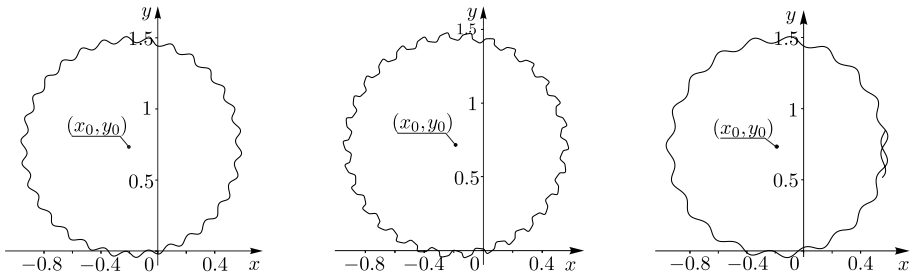

a) $\Omega_\psi = 0.52$ rad/s, $x_0 = -0.186$ m, $y_0 = 0.73$ m

b) $\Omega_\psi = 0.21$ rad/s, $x_0 = -0.186$ m, $y_0 = 0.71$ m

c) $\Omega_\psi = 1.34$ rad/s, $x_0 = -0.19$ m, $y_0 = 0.73$ m

FIGURE 3. Examples of trajectories of point P for $\alpha = 0.5$ rad, $\varphi_0 = 0.3$ rad: a) $N = 0$, $T = 0.4$ s, $p = 1, q = 30$, the trajectory becomes closed after q periods of control, b) $N = 5$, $T = 1$ s, $p = 1, q = 30$, the trajectory becomes closed after q periods of control, c) $N = 0$, $T = 0.25$ s, the trajectory is quasi-periodic and bounded

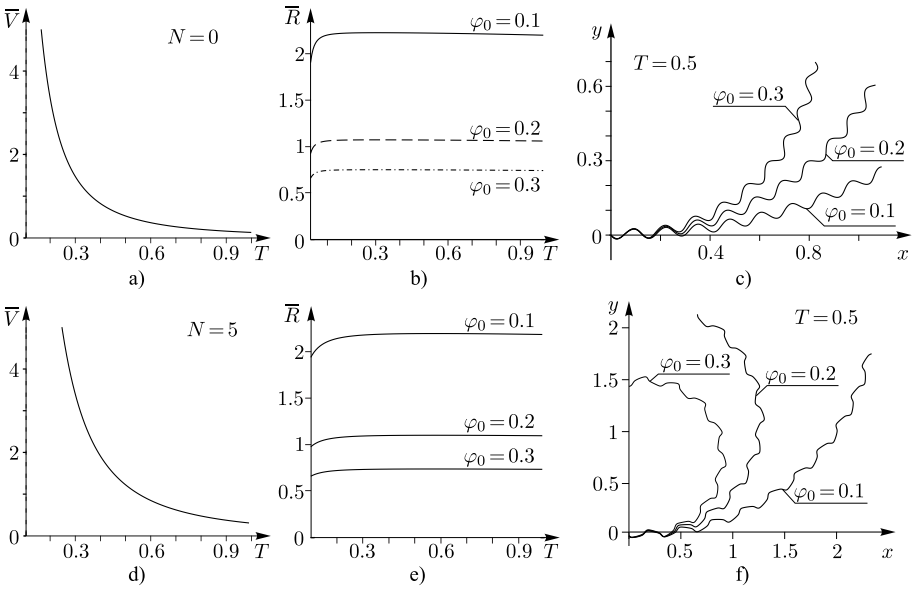

FIGURE 4. a), d) Graphs showing the dependence of the average linear velocity $\bar{V}(T)$ of motion along a circle, b), e) the average distance $\bar{R}(T)$ of point P on (x_0, y_0) depending on period T, and c), f) the trajectories of point P at $\alpha = 0.5$ rad, $\varphi_0 = 0.1$ rad, $\varphi_0 = 0.2$ rad, $\varphi_0 = 0.3$ rad and $N = 0$ (above), $N = 5$ (below)

Fixing, for example, the parameters N, T and φ_0, one can numerically determine the value of α at which for the chosen k_* relation (3.2) is satisfied. If for the found parameters the corresponding coefficient $A_{k_*} \neq 0$, the trajectory is *unbounded*.

Figure 5 shows examples of such trajectories for $k_* = -1$ and the corresponding closed trajectories defined by relation (2.18) (in the reference frame moving with velocity V_*).

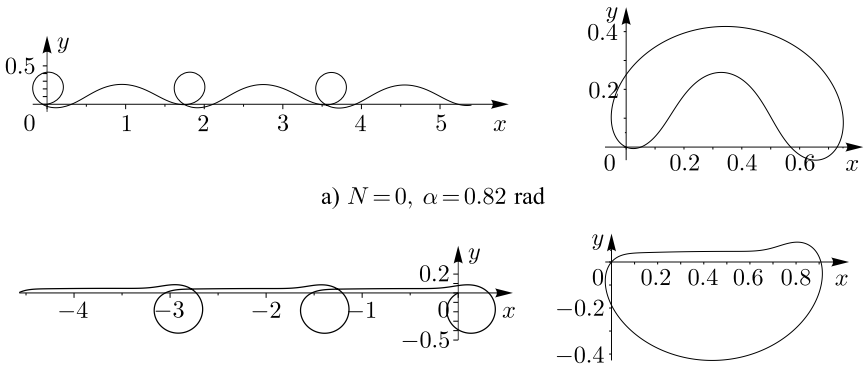

a) $N = 0$, $\alpha = 0.82$ rad

b) $N = 5$, $\alpha = 0.496$ rad

FIGURE 5. Trajectories of point P for $k_* = -1$ ($\Omega_\psi = \Omega$), in the fixed reference frame (left) and the reference frame moving with velocity V_0 (right). Parameters of the control function: $T = 0.05$ s, $\varphi_0 = 0.5$ rad. Characteristics of the trajectory: a) $\psi_* = 1.12$ rad, $V_0 = 36$ m/s; b) $\psi_* = 2.54$ rad, $V_0 = 30.5$ m/s

The resonant parameters of the control function which correspond to the *bounded* trajectory of the system are defined from relation (3.2) under the additional condition $V_* = 0$. We note that for specific mass-geometric parameters of the roller racer this problem may or may not have a solution in the general case.

Of all values of k_* we consider in more detail $k_* = 0$ because in this case equation (3.2) reduces to searching for values of the parameters of the control function at which $\Omega_\psi = 0$.

3.3.1. *The case* $\boldsymbol{k_* = 0}$. In [25] it is shown analytically that in the case of control action $\varphi(t)$ of the form (3.1) with $\varphi_0 = 0$ the function F_T (2.3) is T-periodic with zero average value over a period. According to (2.5), this implies that for $\varphi_0 = 0$, no matter what the value of the other parameters of the control function (3.1), the angular velocity is $\Omega_\psi = 0$.

Thus, according to (3.2), it suffices to fix the value $\varphi_0 = 0$ in the control (3.1) in order to obtain a resonance at $k_* = 0$.

In [25], it is also proved that, when $\varphi_0 = 0$ (and hence when $k_* = 0$), the following relations hold for the coordinates $(\tilde{x}, \tilde{y})$ of the point of attachment P of the platforms of the roller racer in the reference frame $O\tilde{x}\tilde{y}$ rotated by angle ψ_*

(2.17) relative to the inertial reference frame Oxy:

$$\tilde{x}(t) = V_0 t + X(t), \quad \tilde{y}(t) = Y(t),$$
$$X(t) = X(t + T/2), \quad Y(t) = Y(t + T),$$

where $V_0 = V_*$ with $k_* = 0$ is the average velocity of the straight-line motion, which is expressed analytically in terms of the integral

$$V_0 = \frac{2}{T}\int_0^{T/2}\Big(Q(t)\cos\psi_T(t) - c_1\frac{Q(t)\sin\varphi(t) - c_2\dot{\varphi}(t)}{c_1\cos\varphi(t) + c_2}\sin\psi_T(t)\Big)dt. \tag{3.3}$$

The value of $\psi_T(t)$ is determined from relation (2.5) with $\Omega_\psi = 0$:

$$\psi_T(t) = \int_0^t F_T(\tau)d\tau - \frac{1}{T}\int_0^T d\tau\int_0^\tau F_T(z)dz.$$

Examples of unbounded trajectories of point P for different values of the parameters of the control function with $V_0 \neq 0$ are shown in Fig. 6.

When $V_0 = 0$, the point of attachment P of the platforms moves along a *bounded* self-intersecting trajectory (since $\Omega_\psi = 0$). Examples of such trajectories for different parameters of the control function are shown in Fig. 7.

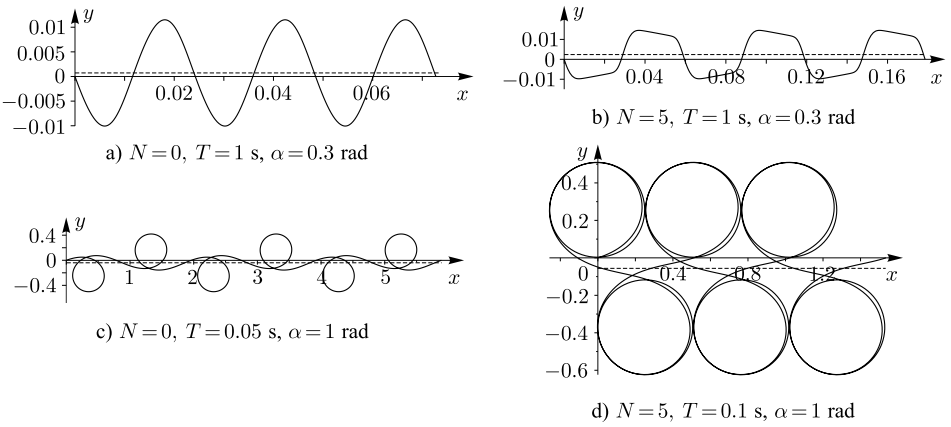

FIGURE 6. Trajectories of the point of attachment P of the platforms for $k_* = 0$ ($\varphi_0 = 0$, $\Omega_\psi = 0$). Parameters of the trajectory: a) $\psi_* = 0.00018$ rad, $V_0 = 0.024$ m/s, $y_0 = 0.00072$ m; b) $\psi_* = 0.00025$ rad, $V_0 = 0.0595$ m/s, $y_0 = 0.00239$ m; c) $\psi_* = 0.00028$ rad, $V_0 = 39.3$ m/s, $y_0 = -0.041$ m; d) $\psi_* = 0.0008$ rad, $V_0 = 5.11$ m/s, $y_0 = -0.057$ m

4. Analysis of the average velocity of motion for $k_* = 0$

Next, we estimate the influence of the control parameters and the mass-geometric characteristics of the system on the value of the average velocity V_0 (3.3). This estimate allows us to form a control ensuring the maximal velocity of motion for the prescribed mass-geometric characteristics of the roller racer or, alternatively, to

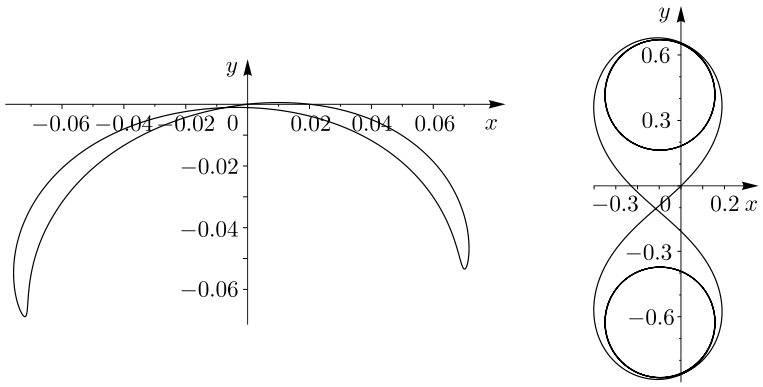

a) $N = 0$ b) $N = 5$

FIGURE 7. Self-intersecting trajectories of point P for $k_* = 0$ ($\varphi_0 = 0$, $\Omega_\psi = 0$). Parameters of the control function: a) $N = 0$, $T = 2$ s, $\alpha = 2.465$ rad; b) $N = 5$, $T = 0.05$ s, $\alpha = 0.9998$ rad

optimize the design for the given technically bounded controls. We consider these cases separately.

4.1. Fixed mass-geometric parameters. Consider the dependence of the average velocity of motion of the roller racer V_0 (3.3) on the control parameters (3.1).

Without loss of generality, in this case, we can assume period T to be equal to unity. This corresponds to the choice of units for measuring time and follows from invariance of equations (2.1) and (2.2) under the change of variables

$$t \to Tt, \quad v_1 \to v_1/T, \quad \mu_1 \to \mu_1/T, \quad \mu_2 \to \mu_2/T. \tag{4.1}$$

Thus, a change in the period is equivalent to scaling the friction coefficient. The dependence of velocity V_0 on the friction coefficient will be considered below in Section 4.2.

Figure 8 shows the surface of the dependence $V_0(\alpha, N)$ for $T = 1$ s, obtained by numerical simulation with the parameters (2.19).

The resulting dependences allow the following conclusions:

- *the average velocity of motion V_0 increases with an increase in the value of N;*
- *there exists an optimal value of the amplitude α of the function $\varphi(t)$ for the prescribed mass-geometric parameters of the roller racer at which the average velocity of motion V_0 is maximal.*

For example, when $\varphi_0 = 0$, $T = 1$ s and $N = 0$, the maximal value of the velocity $V_0 = 0.247$ m/s is reached at $\alpha = 1.384$ rad, and when $N = 5$, the maximal velocity $V_0 = 0.439$ m/s is reached at $\alpha = 1.136$ rad.

Thus, the maximal velocity of motion can be reached at some optimal value of the amplitude of the control action and at the largest possible value of N, which

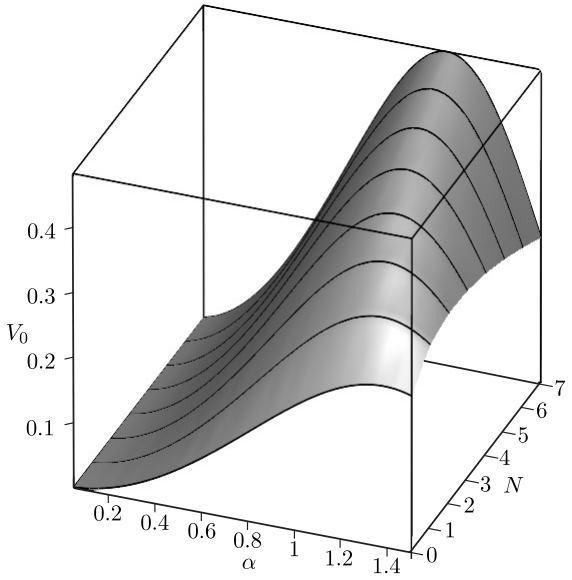

FIGURE 8. Dependence $V_0(N, \alpha)$ for $\varphi_0 = 0$, $T = 1$ s and the parameters (2.19)

in practice corresponds to the rotation of the second platform relative to the first platform with the maximal angular acceleration.

The largest possible value of N depends on the performance capabilities of the roller racer. Besides, in carrying out experimental investigations, account should be taken of the fact that, as the value of N increases, so do the constraint reaction forces, see (1.5). This can lead to slipping at the points of contact with the plane.

4.2. Fixed control parameters.

4.2.1. *Dependence of the motion velocity of the roller racer on the mass of the second platform.* In this section, we investigate the dependence of the velocity of the straight-line motion of the roller racer on the mass of the second platform without changes in the control parameters. For definiteness, we choose the following fixed control parameters:

$$N = 5, \quad \alpha = 0.9 \text{ rad}, \quad \varphi_0 = 0 \text{ rad}, \quad T = 1 \text{ s}. \tag{4.2}$$

As was noted above, the design features of the full-scale specimen of the roller racer allow this to be done by adding weights into special compartment placed on the second platform. In this case, the value of the moment of inertia I_{20} will change as well. But, since its changes are completely determined by changes in the mass, we will not present the corresponding surface in the space (m_2, I_{20}, V_0), present only its projection onto the plane (m_2, V_0) for the fixed control parameters (4.2).

The resulting dependence $V_0(m_2)$ is shown in Fig. 9, which implies that *the average velocity of motion V_0 increases with an increase in the mass of the second*

platform without changes in the geometric parameters of the roller racer to some optimal value.

Thus, despite the fact that the possibility of slipping diminishes as the mass of the system increases, there exists an optimal value of the mass that corresponds to the largest possible (with other parameters specified) value of the average velocity.

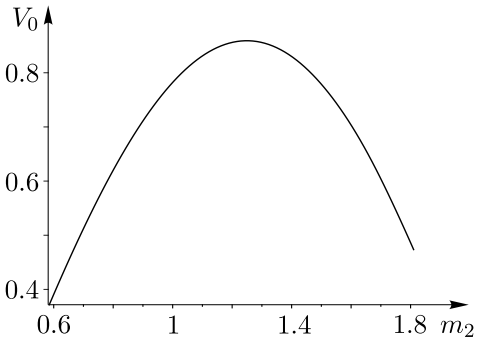

FIGURE 9. Graph showing the dependence $V_0(m_2)$ of the velocity of motion of the roller racer with the control parameters (4.2). As initial values of the mass and the moment of inertia of the second platform we have taken the values (2.19)

4.2.2. *Dependence of the velocity of motion of the roller racer on the friction coefficient.* Another parameter on which velocity V_0 depends considerably is the reduced viscose friction coefficients μ (in this case we assume $\mu_1 = \mu_2 = \mu$). This is a parameter that can be determined experimentally and depends on the characteristics of the materials of the wheels of the roller racer and the surface on which it rolls.

Figure 10a shows numerically calculated dependences of the velocity of motion of the roller racer on the friction coefficient $V_0(\mu)$ for two different controls, with $N = 0$ and $N = 5$. As one would expect, *the larger the friction coefficient, the smaller the velocity of motion* V_0.

From the transformation (4.1) it follows that the dependence $V_0(T)$ with μ fixed is the same as $V_0(\mu)$ with T fixed. Thus, if the reduced viscose friction coefficients are predetermined (for example, in the experiment), *to increase the velocity* V_0*, it is necessary to decrease the value of period* T, see Fig. 10b.

5. Experimental results

At the Laboratory of Mobile Systems (Kalashnikov Izhevsk State Technical University), a prototype of the roller racer has been built using the equipment of the Common Use Center of the Udmurt State University to verify the simulation results.

The values of the mass-geometric parameters were calculated from the 3D model of the roller racer in the software product Solid Works (Fig. 11), see (2.19).

The motion of the prototype was performed on a plane surface. To film the trajectory and to recover the relative angular position of the platforms, light-reflecting

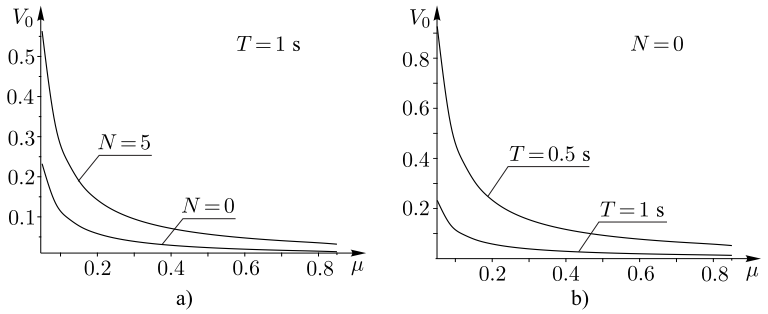

FIGURE 10. Graph showing the dependence of the velocity of motion on the reduced viscose friction coefficients $V_0(\mu)$ of the roller racer for $\alpha = 0.4$ rad, $\varphi_0 = 0$ and the parameters (2.19): a) for $N = 0$ and $N = 5$ with $T = 1\,\mathrm{s}$, b) for $N = 0$ with $T = 0.5\,\mathrm{s}$ and $T = 1\,\mathrm{s}$

markers of the motion capture system VICON were placed on the large (1) and the small (2) platform (see Fig. 11a).

In the experiments, account was taken of restrictions on the maximal relative turning angle of the platforms. For this specimen, the maximal angular displacement is $\alpha = 1.4$ rad.

Furthermore, the torque curves and the speed performance of the servodrive used are technically limited and allow turning the platforms with control at $N < 6$.

Another design feature that cannot be disregarded is the deviation of the experimental value of φ_0 from the prescribed one. Specifically, in the course of experiments, we obtained from the coordinates of the markers the small value $\varphi_0 \backsim 10^{-2}$ rad for the input value $\varphi_0 = 0$. As shown above, this leads to a deviation from the generally rectilinear motion.

In the course of experimental investigations, as in the course of simulations, a comparison was made of the average velocity of motion of the roller racer, which was reached by the prototype in the process of motion from the state of rest. In

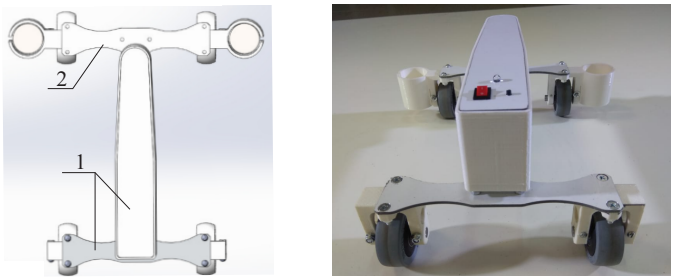

FIGURE 11. a) 3D model and b) picture of the full-scale specimen of the roller racer

recovering the experimental trajectories of motion, the stage of acceleration was not taken into account.

In addition, to exclude random factors such as the initial position and local surface irregularities, for each set of control parameters and for each design of the roller racer, a series of eight experiments were carried out. Later, for each series, we calculated averaged values and the corresponding confidence intervals.

The experimental verification of the dependence of the velocity of motion of the roller racer on the control parameters was performed for two configurations: with parameters (2.19) and with additional weights on the second platform. The corresponding parameters have the following values:

$$m_2 = 0.853 \text{ kg}, \quad a_2 = 0.0015 \text{ m}, \quad c_2 = 0.044 \text{ m}, \tag{5.1}$$
$$I_{02} = 0.0077 \text{ kg} \cdot \text{m}^2, \quad b_2 = 0.0078 \text{ m}.$$

5.1. Straight-line motion. A typical trajectory of the straight-line motion of the point of contact, P, of the platforms of the roller racer and the corresponding variation curve of the average velocity of motion are shown in Fig. 12.

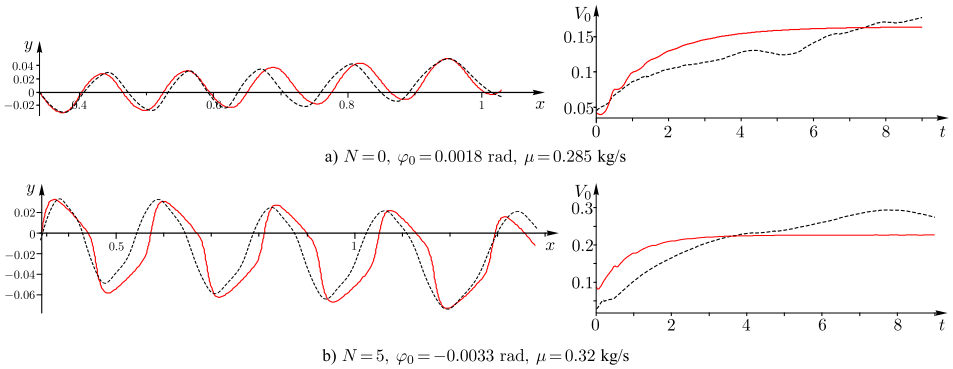

FIGURE 12. Comparison of the experimental results (black dashed curves) and simulation (red solid curves) of the motion of the roller racer for the parameters (2.19) and the control parameters $\alpha = 0.7$ rad, $T = 1$ s, $N = 0$ (a) and $N = 5$ (b). Left: trajectories of motion. Right: the corresponding variation curves of the average velocity of motion

The observed deviation of the experimental trajectory from generally rectilinear motion is due to the above-mentioned deviation of the experimentally obtained value of φ_0 from the prescribed value. Specifically, for the prototype under consideration, at the prescribed value $\varphi_0 = 0$ the experimentally observed value was $\varphi_0 = 0.0018$ rad for $N = 0$ and $\varphi_0 = -0.0033$ rad for $N = 5$. This value was taken into account in simulation, and, as can be seen from the pattern of the trajectory obtained according to the simulation results, the trajectory repeats qualitatively the experimental results.

The value of the reduced viscose friction coefficients μ shown in Fig. 12 corresponds to the theoretical curve and was chosen in such a way that the deviation of the theoretical trajectory from the experimental one was minimal. We note that, in practice, the process of determining the values of the coefficients of viscous friction is rather time-consuming, and for an exact quantitative agreement of the model it is necessary to carry out experiments for each pair of materials and for each regime of motion. This is why in this paper we verified the agreement of the experimental data with the theoretical data in the range of values of the coefficients $\mu = 0.2 - 0.35$ kg/s [29]. The tabular values of the rolling friction coefficient for materials similar to those used in this paper lie in this range.

Local surges in the variation curve of the velocity (see Fig. 12, right) are caused by errors of equipment, errors of differentiation of discrete data, and by local irregularities, which decelerate or accelerate the motion of the prototype in some path segments. The behavior of the velocity of motion of the roller racer, including that in the initial stage, before reaching a periodic solution, is in qualitative agreement with numerical results.

1°. To verify the dependence of the velocity of motion along a straight line on the control parameters (N and α), a series of experiments for the roller racer with the parameters (2.19) and the following sets of control parameters were carried out:

1. $N = 0$, $T = 1$ s for $\alpha = 0.7$ rad and $\alpha = 0.9$ rad;
2. $N = 5$, $T = 1$ s for $\alpha = 0.5$ rad and $\alpha = 0.7$ rad.

Figure 13 shows the results of the experiments and the numerically calculated curves of dependence $V_0(N, \alpha)$ (see also Fig. 8) for values of the friction coefficient corresponding to the boundaries of the above-mentioned range (shown as dashed lined). In the chosen range of values of α (smaller than the optimal one at the prescribed value of N) the obtained experimental results qualitatively confirm the theoretical results: as the parameters of the control function, α and N, increase, so does the average velocity of the straight-line motion of the roller racer. Note that the experimental values, including the confidence intervals, lie inside the regions bounded by the theoretical curves. This implies that the proposed model with viscous friction provides an adequate qualitative and quantitative description of the straight-line motion of the roller racer.

2°. To investigate the influence of the mass-geometric parameters on the velocity of the prototype of the roller racer, a series of additional experiments were conducted at $N = 0$, $T = 1$ s, $\varphi_0 = 0$ $\alpha = 0.7$ rad and $\alpha = 0.9$ rad for the roller racer with the parameters (5.1).

The corresponding experimental results shown in Fig. 14 confirm qualitatively the theoretical results: as the mass of the second platform increases, so does the average velocity of the straight-line motion of the roller racer.

The experimental values, including the confidence intervals, lie inside the regions bounded by curves which correspond to the boundary values of the friction coefficient. This indicates a quantitative agreement between theory and experiment. The small confidence intervals (for example, at $\alpha = 0.9$ rad and at the parameters (5.1)) correspond to good repeatability of the experimental results.

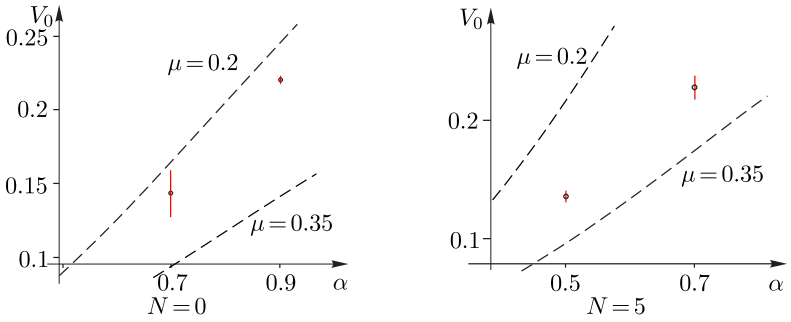

FIGURE 13. Dependences of the velocity of motion of the prototype of the roller racer with the parameters (2.19) on the parameters of the control function N and α with $T = 1$ s (the experimental values with confidence intervals are shown). The dashed line shows the graphs obtained numerically for different values of the friction coefficient.

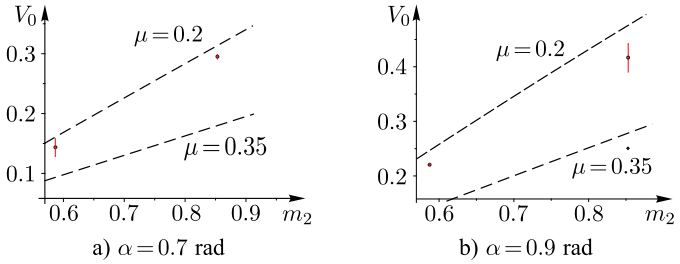

FIGURE 14. Comparison of experimental and theoretical values of the velocity of motion of the roller racer in the case of different masses of the second platform for $\alpha = 0.7$ rad (a) and $\alpha = 0.9$ rad (b), $N = 0$, $T = 1$ s, $\varphi_0 = 0$. The theoretical curves $V_0(m_2)$ (shown as dashed lines) are plotted at the same parameters for two values of the coefficients of viscous friction $\mu = 0.2$ kg/s and $\mu = 0.35$ kg/s.

5.2. Motion along a circle. A typical trajectory of the point of contact, P, of the platforms of the roller racer along a circle and the corresponding variation curve of the average velocity of motion are shown in Fig. 15.

The local oscillations in the variation curve of the angular velocity are caused by surface irregularities, which decelerate or accelerate the motion of the prototype in some path segments. The behavior of the velocity of motion of the roller racer, including that in the initial stage, is in qualitative agreement with the numerical results. The value of the friction coefficient μ shown in Fig. 15 corresponds to the theoretical curve and has been chosen in such a way that the deviation of the theoretical trajectory from the experimental one is minimal.

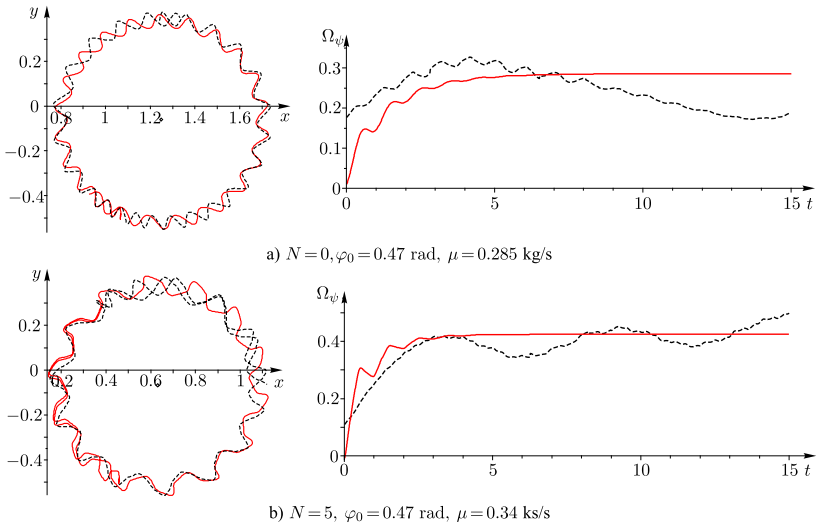

FIGURE 15. Comparison of the results of experiments (black dashed curves) and modeling (red solid curves) of the motion of the roller racer along a circle for the parameters (2.19) and the control parameters $\alpha = 0.7$ rad, $T = 1$ s, $N = 0$ (a) and $N = 5$ (b). Left: trajectories of motion. Right: the corresponding variation curves of the angular velocity of motion $\Omega_\psi(t)$

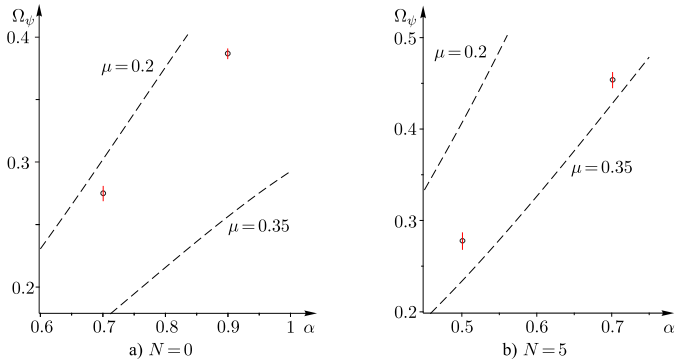

FIGURE 16. Dependences of the angular velocity of motion Ω_ψ of the prototype of the roller racer with the parameters (2.19) on the parameters of the control function N and α at $T = 1$ s (the experimental values with confidence intervals are shown). The dashed lines represent the graphs obtained numerically at the same parameters for different values of the friction coefficient.

To verify the dependence of the angular velocity of motion along a circle on the control parameters (N and α), a series of experiments were conducted for the roller racer with the parameters (2.19) and the following sets of control parameters:

1. $N = 0$, $T = 1$ s, $\varphi_0 = 0.47$ rad with $\alpha = 0.7$ rad and $\alpha = 0.9$ rad;
2. $N = 5$, $T = 1$ s, $\varphi_0 = 0.47$ rad with $\alpha = 0.5$ rad and $\alpha = 0.7$ rad.

Figure 16 shows the results of experiments and the numerically calculated curves of dependence $V_0(N, \alpha)$ for values of the friction coefficient which correspond to the boundaries of the above-mentioned range (shown as dashed lines). In the chosen range of values of α (smaller than the optimal one at the prescribed value of N), the obtained experimental results confirm qualitatively the theoretical results: as the parameters of the control function, α and N, increase, so does the angular velocity of motion of the roller racer along a circle. The experimental values, including the confidence intervals, lie inside the regions bounded by these curves. Thus, in the case of motion along a circle (as in the case of motion along a straight line) the proposed model with viscous friction provides an adequate qualitative and quantitative description of the motion of the roller racer.

Conclusion

In this paper, we have investigated the controlled motion of a roller racer on a plane depending on the control parameters and the mass-geometric parameters of the system. It is shown that, for the chosen periodic control function, there exists a bounded (along a circle) and an unbounded (along a straight line) motion of the system. Unbounded motion corresponds to the resonant case which takes place at zero average value of the control function.

It is shown that the average velocity of the straight-line motion increases with decreasing period of the control function and with increasing rapidity of motion (the maximal angular velocity of rotation of the platforms relative to each other). Furthermore, for the prescribed mass-geometric parameters of the roller racer there exists an optimal value of the amplitude α of the relative oscillations of the platforms at which the average velocity of motion, V_0, is maximal. These dependences have been determined theoretically and confirmed experimentally.

In this paper, it is shown experimentally that the model of nonholonomic motion chosen to describe the system and taking the viscous friction torque into account provides an adequate description of the observed motion. The trajectory of the full-scale specimen of the roller racer is in qualitative agreement with the theoretically calculated trajectory.

The design of the prototype of the roller racer used in the experiments allows changes in the mass of the second platform. Also, the changes occur in the position of the center of the system's mass and in the corresponding moments of inertia. In this paper, it is shown theoretically and experimentally that, as the mass of the second platform increases to some optimal value, so does the velocity of motion of the roller racer.

To optimize the design of the roller racer, it would be interesting to experimentally investigate the dependence of the velocity of its motion along a straight

line on the mass of the second platform without changes in its moment of inertia and, alternatively, the dependence of the velocity on the moment of inertia of the second platform without changes in its mass.

It would also be of special interest to optimize the design of the roller racer and the control actions taking into account both the results obtained in this paper and a possible switching of one or several wheels of the roller racer to the sliding mode. This requires an analysis of constraint reactions arising at the points of contact of the wheels with the plane of motion.

Acknowledgments. The authors thank V. Krasnova for assistance in conducting the experiments.

The work of A. A. Kilin (Sections 1, 2) was carried out within the framework of the state assignment of the Ministry of Science and Higher Education of Russia (FEWS-2020-0009). The work of T. B. Ivanova (Sections 3) was performed at the Ural Mathematical Center (Agreement No 075-02-2024-1445). The work of Y. L. Karavaev (Sections 3) and the work of K. S. Yefremov (Section 4) were carried out within the framework of the state assignment of the Ministry of Science and Higher Education of Russia (FZZN-2020-0011).

References

1. A. V. Borisov, A. A. Kilin, I. S. Mamaev, *On the Hadamard–Hamel problem and the dynamics of wheeled vehicles*, Regul. Chaotic Dyn. **20**(6) (2015), 752–766.
2. I. A. Bizyaev, *The inertial motion of a roller racer*, Regul. Chaotic Dyn. **22**(3) (2017), 239–247.
3. I. A. Bizyaev, A. V. Borisov, I. S. Mamaev, *Exotic dynamics of nonholonomic roller racer with periodic control*, Regul. Chaotic Dyn. **23**(7) (2018), 983–994.
4. A. V. Borisov, A. A. Kilin, I. S. Mamaev, *Invariant submanifolds of genus 5 and a Cantor staircase in the nonholonomic model of a snakeboard*, Int. J. Bifurcation Chaos Appl. Sci. Eng. **29**(3) (2019), 1930008.
5. A. V. Borisov, I. S. Mamaev, A. A. Kilin, I. A. Bizyaev, *Qualitative analysis of the dynamics of a wheeled vehicle*, Regul. Chaotic Dyn. **20**(6) (2015), 739–751.
6. E. M. Artemova, I. A. Bizyaev, *Dynamics of a multilink wheeled vehicle: partial solutions and unbounded speedup*, Int. J. Non-Linear Mech. (2024), 104774.
7. A. Bravo-Doddoli, L. C. García-Naranjo, *The dynamics of an articulated n-trailer vehicle*, Regul. Chaotic Dyn. **20** (2015), 497–517.
8. E. M. Artemova, A. A. Kilin, *A nonholonomic model and complete controllability of a three-link wheeled snake robot*, Russ. J. Nonlinear Dyn. **18**(4) (2022), 681–707.
9. B. Stückler, *Über die Differentialgleichungen für die Bewegung eines idealisierten Kraftwagens*, Ing.-Arch. **20**(5) (1952), 337–356.
10. B. Stückler, *Über die Berechnung der an rollenden Fahrzeugen wirkenden Haftreibungen*, Ing.-Arch. **23**(4) (1955), 279–287.
11. O. Bottema, *Die Bewegung eines einfachen Wagenmodells*, Z. Angew. Math. Mech. **44**(12) (1964), 585–593.
12. Y. Rocard, *L'instabilité en mécanique: automobiles, avions, ponts suspendus*, Collection Evolution des sciences, Masson, Paris, 1954.
13. J. Ostrowski, A. Lewis, R. Murray, J. Burdick, *Nonholonomic mechanics and locomotion: The snakeboard example*, Proceedings of the 1994 IEEE International Conference on Robotics and Automation, IEEE, San Diego, CA, USA, 1994.
14. F. Bullo, A. D. Lewis, *Kinematic controllability and motion planning for the snakeboard*, IEEE Transactions on Robotics and Automation **19**(3) (2003), 494–498.

15. E. Shammas, M. De Oliveira, *Motion planning for the snakeboard*, The International Journal of Robotics Research **31**(7) (2012), 872–885.
16. Y. G. Martynenko, *Motion control of mobile wheeled robots*, J. Math. Sci. **147**(2) (2007), 6569–6606.
17. A. V. Borisov, I. S. Mamaev, *Symmetries and reduction in nonholonomic mechanics*, Regul. Chaotic Dyn. **20** (2015), 553–604.
18. A. S. Kuleshov, *Further development of the mathematical model of a snakeboard*, Regul. Chaotic Dyn. **12** (2007), 321–334.
19. P. Krishnaprasad, D P. Tsakiris, *Oscillations, SE (2)-snakes and motion control: A study of the roller racer*, Dyn. Syst. **16**(4) (2001), 347–397.
20. P. Cheng, E. Frazzoli, V. Kumar, *Motion planning for the roller racer with a sticking/slipping switching model*, Proceedings 2006 IEEE International Conference on Robotics and Automation, 2006. ICRA 2006, IEEE, Orlando, FL, USA, 2006, 1637–1642.
21. I. A Bizyaev, I. S. Mamaev, *Roller Racer with varying gyrostatic momentum: Acceleration criterion and strange attractors*, Regul. Chaotic Dyn. **28**(1) (2023), 107–130.
22. O. Halvani, Y. Or, *Nonholonomic dynamics of the Twistcar vehicle: asymptotic analysis and hybrid dynamics of frictional skidding*, Nonlinear Dyn. **107**(4) (2022), 3443–3459.
23. E. A. Mikishanina, *Qualitative analysis of the dynamics of a trailed wheeled vehicle with periodic excitation*, Russ. J. Nonlinear Dyn. **17**(4) (2021), 437–451.
24. E. A. Mikishanina, *The problem of acceleration in the dynamics of a double-link wheeled vehicle with arbitrarily directed periodic excitation*, Theor. Appl. Mech. **50**(2) (2023), 205-–221.
25. K. S. Yefremov, T. B. Ivanova, A. A. Kilin, Y. L. Karavaev, *Theoretical and experimental investigations of the controlled motion of the roller racer*, 2020 International Conference Nonlinearity, Information and Robotics (NIR), IEEE, Innopolis, Russia, 5 p., 2020.
26. A. A. Kilin, Y. L. Karavaev, K. S. Yefremov, *Experimental investigations of the controlled motion of the roller racer robot*, in: D. Chugo, M. O. Tokhi, M. F. Silva, T. Nakamura, K. Goher (eds.), *Robotics for Sustainable Future. CLAWAR 2021*, Lect. Notes Netw. Syst. 324, 428–437, Springer, Cham, 2022.
27. J. W. Strutt, *Some general theorems relating to vibrations*, Proc. Lond. Math. Soc. **1**(1) (1871), 357–368.
28. A. V. Borisov, A. A. Kilin, I. S. Mamaev, *How to control the Chaplygin ball using rotors. II*, Regul. Chaotic Dyn. **18** (2013), 144–158.
29. I. V. Kragelsky, M. N. Dobychin, V. S. Kombalov, *Friction and Wear: Calculation Methods*, Elsevier, 2013.

ТЕОРИЈСКА И ЕКСПЕРИМЕНТАЛНА ИСТРАЖИВАЊА КОНТРОЛИСАНОГ КРЕТАЊА РОЛЕР-РЕЈСЕРА

Реиме. У овом раду бавимо се проблемом контролисаног кретања ролер-рејсера по равни. Претпостављамо да је угао између платформи дата периодична функција времена (управљачка функција), а услови неклизања (нехолономно ограничење) и силе вискозног трења делују у тачкама контакта точкова и равни. У овом случају све трајекторије редукованог система асимптотски теже ка периодичном решењу. У овом раду показујемо да за изабрану периодичну управљачку функцију постоји кретање система које је ограничено (дуж круга) и неограничено (дуж праве). Неограничено кретање одговара резонантном случају који се одвија при нултој просечној вредности управљачке функције. Истражује се теоријска зависност путање и брзине ролер-рејсера од његових параметара и параметара изабране управљачке функције. Ове зависности су потврђене експериментално.

Ural Mathematical Center
Udmurt State University
Izhevsk
Russia
kilin@rcd.ru
https://orcid.org/0000-0003-1358-5960

Ural Mathematical Center
Udmurt State University
Izhevsk
Russia
tbesp@rcd.ru
https://orcid.org/0000-0003-3553-4814

Kalashnikov Izhevsk State Technical University
Izhevsk
Russia
karavaev_yury@istu.ru
https://orcid.org/0000-0002-6679-1293

Kalashnikov Izhevsk State Technical University
Izhevsk
Russia
ks.efremov18@gmail.com
https://orcid.org/0000-0002-8618-7747

(Received 03.12.2024)
(Revised 23.12.2024)
(Available online 25.12.2024)